Fluid Phase Equilibria 274 (2008) 36–43

Contents lists available at ScienceDirect

Fluid Phase Equilibria

journal homepage: www.elsevier.com/locate/fluid

One force field for predicting multiple thermodynamic properties of liquid and vapor ethylene oxide

Xiaofeng Li, Lifeng Zhao, Tao Cheng, Lianchi Liu, Huai Sun*

School of Chemistry and Chemical Technology, Shanghai Jiao Tong University, Shanghai 200240, China

ARTICLE INFO

Article history:
Received 5 March 2008
Received in revised form 24 June 2008
Accepted 24 June 2008
Available online 9 July 2008

Keywords:
Ethylene oxide
Force field
Molecular dynamics
Monte Carlo

ABSTRACT

Molecular dynamics (MD) and Monte Carlo (MC) methods were applied to calculate thermodynamic properties of ethylene oxide in liquid and vapor phases. The calculations were based on the TEAM force field that was derived based on quantum mechanics data, liquid density and heat of vaporization. Without any modification, the force field was applied to predict various thermodynamic properties including vapor–liquid coexistence curves, critical points, second virial coefficient, isothermal compressibility, surface tensions, shear viscosities and thermal conductivities. Good agreements between the calculated and experimental data are obtained for most properties predicted. Although some of the deviations require further investigation, the force field appears to be transferable for predicting multiple thermodynamic properties.

1. Introduction

In this paper, we report predictions of multiple thermodynamic properties of ethylene oxide in liquid and vapor phases based on TEAM force field [1]. This work was initiated as a response to the 4th Industrial Fluid Property Simulation Challenge (IFPSC) [2]. The main purpose of this work, as clearly stated in the IFPSC committee announcement, is to test the transferability of methods and force fields to a wide variety of properties for a given molecule.

Ethylene oxide is an important industrial chemical used as an intermediate in the production of ethylene glycol and other chemicals. It is flammable, reactive, explosive and toxic so special care must be considered in its use. These features make it dangerous and expensive to measure its properties experimentally. Molecular simulation offers an attractive alternative to laboratory studies. Several models have been developed to calculate molecular properties of ethylene oxide in gas and liquid phases. For examples, Wielopolski and Smith [3] have developed a united-atom model with the objective to study the dielectric properties of liquid ethylene oxide; Krishnamurthy et al. [4] have estimated the Henry's law constants and solubility of several non-polar molecules in ethylene oxide; Wu et al. [1b] have developed force field parameters to calculate the Henry's law constants of small molecules in ethylene oxide; Mountain [5] has examined three existing force field models of increasing complexity and found out that only the polarizable model can reproduce both gas phase and liquid phase properties of ethylene oxide.

In this work, as a part of on-going project for developing a new all-atom TEAM force field, ethylene oxide was parameterized to predict thermodynamic properties of this molecule in liquid and vapor phases. There were several motivations beside "to win the competition". We wanted to test if a force field developed using a set of basic data can be used to predict a broad range of physical and thermodynamic properties. How to make such as transferable parameters using the basic data was an interconnected question. In addition, we wanted to assess available molecular simulation methods for predicting various properties.

2. Force fields and simulation methods

The TEAM force field is a collection of all-atom force fields parameterized based on the same *ab initio* and empirical data but cast in several different force field types. In this work, the force field is in AMBER functional form:

$$E = \sum_{\text{bond}} K_b(b-b_0)^2 + \sum_{\text{angle}} K_\theta(\theta-\theta_0)^2 + \sum_{\text{dihedral}} \frac{K_\phi}{2}[(1+\cos(n\phi-\phi_0))] + \sum_{\text{improper}} \frac{K_\chi}{2}[(1+\cos(n\chi-\chi_0))] + \sum_{\text{non bond}} \left\{ \varepsilon_{ij}\left[\left(\frac{R_{ij}^0}{r_{ij}}\right)^{12} - 2\left(\frac{R_{ij}^0}{r_{ij}}\right)^{6}\right] + \frac{q_i q_j}{r_{ij}} \right\} \quad (1)$$

* Corresponding author. Tel.: +86 21 5474 8987 601; fax: +86 21 5474 1297.
E-mail address: huaisun@sjtu.edu.cn (H. Sun).

0378-3812/$ – see front matter © 2008 Elsevier B.V. All rights reserved.
doi:10.1016/j.fluid.2008.06.021

Table 1
Atomic partial charges and molecular dipole moments of ethylene oxide calculated using the ESP and PCM/ESP models

	Atomic charge (e)			Dipole (Debye)
	C	H	O	
ESP	−0.083	0.106	−0.259	1.98
PCM/ESP	−0.076	0.117	−0.317	2.33

The experimental dipole moment of the molecule in gas phase is 1.90 Debye

The non-bond interactions are between atoms either in different molecules or in the same molecule but separated by at least three consecutive bonds (1–4 and beyond interactions). 1–4 scaling factor for the LJ interaction is 0.5 and for the electrostatic interaction is 0.833. Partial charges are used for the electrostatic interactions. The LJ parameters for unlike atoms are constructed using the Lorentz–Berthelot combination rules:

$$\varepsilon_{ij} = \sqrt{\varepsilon_i \varepsilon_j}$$
$$R_{ij}^0 = \frac{R_i^0 + R_j^0}{2} \quad (2)$$

A hybrid procedure consisting of *ab initio* and empirical parameterization methods [1] was used in developing the parameters. In order to use the force field for condensed phases, the charge parameters were derived from the electrostatic potential calculated using the polarizable continuum solvent (PCM) model. As shown in Table 1, the molecular dipole moment calculated using the PCM model is 17% larger than that obtained without the polarization. The later is in close agreement with the experimental data measured for the molecule in gas phase.

In order to reduce the adjustable parameters, the initial LJ parameters were derived using a test particle method. A neon atom was used as the test particle to probe the hyper-surfaces of the interaction energies between the neon atom and the ethylene oxide molecule. The energies were sampled by placing the neon atom along five paths as shown in Fig. 1. The distances between the neon atom and the closest atom of the molecule were between 3.0 and 6.0 Å, and the data were collected at an interval of 0.2 Å. These calculations were performed at the MP2/6-311+g(2d,2p) level of theory using Gaussian03 software package [6]. A set of parameters were obtained by fitting the calculated energy data to the LJ function. The parameters (initial LJ parameters) are given in Table 2.

Table 2
Initial and optimized LJ 12-6 parameters for ethylene oxide

Atom	Initial		Final	
	R^0 (Å)	ε (kJ/mol)	R^0 (Å)	ε (kJ/mol)
C	3.2406	1.3304	3.7989	0.5062
O	3.0039	1.7138	3.5215	0.6520
H	2.2238	0.0944	2.6070	0.0360

Table 3
Comparison of structural parameters of experimental measurement [7], quantum mechanics (QM) calculation at the B3LYP/6-31G* level of theory and the molecular mechanics (MM) calculation based on the TEAM force field

Property	Expt.	QM	MM
C–H (Å)	1.085	1.0906	1.0901
C–C (Å)	1.466	1.4694	1.4684
C–O (Å)	1.431	1.4298	1.4290
C–O–C (°)	61.24	61.84	61.83
H–C–H (°)	116.6	115.18	115.58
H–C–O (°)		115.44	115.35
H–C–C (°)		119.72	118.77
H–C–C–H (°)	22	27.13	27.6

With the charge and initial LJ parameters fixed, the valence parameters were derived by fitting the *ab initio* energy, first and second derivatives of the total energy of ethylene oxide at its optimized structure. The calculations were performed at the level of B3LYP/6-31G*. The resulting valence parameters were then combined with the charge and initial LJ parameters to form a complete force field. This force field was subsequently optimized by simultaneously fitting both gas and liquid phase properties of ethylene oxide. Table 3 compares the calculated and experimental data [7] of the structural properties of the molecule. Fig. 2 is a comparison of the calculated and experimental [8] vibrational frequencies. For the liquid phase, the properties used for optimizing the force field were saturated densities and heats of vaporization at 298, 375 and 420 K. Table 4 lists comparisons of the calculated and experimental densities and heats of vaporization of liquid ethylene oxide at these temperatures and saturated vapor pressures. The average deviations of the liquid densities and heats of vaporization are −0.1 and 4.5%, respectively. These results indicate that consistent agreements are obtained using the optimized parameters. The optimized LJ parameters are listed in Table 2 and the valence parameters are

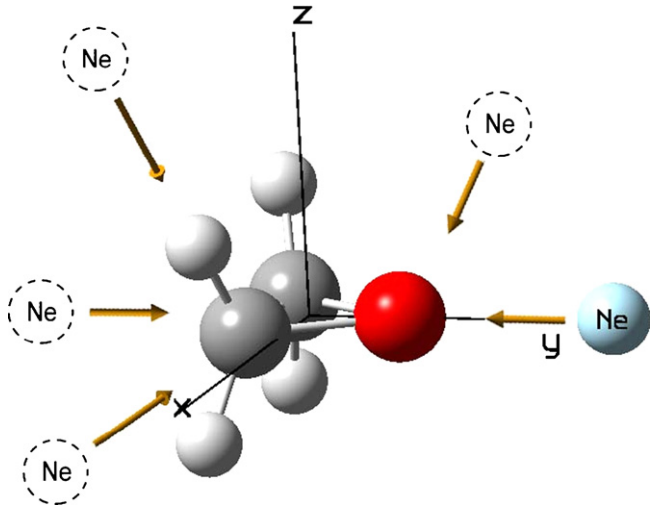

Fig. 1. Test particle sampling of the interactions between neon atom and the ethylene oxide.

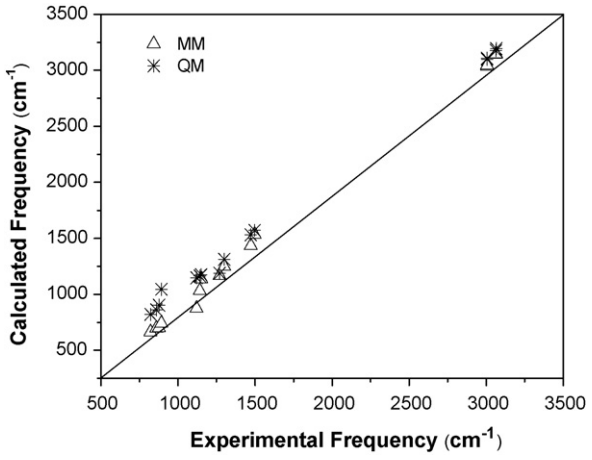

Fig. 2. Comparison of vibrational frequencies of ethylene oxide between calculated and experimental values: (△) molecular mechanics calculation results; (*) quantum mechanics calculation results.

Table 4
Comparison of experimental [10] and calculated densities and heat of vaporization of saturated ethylene oxide liquid in present TEAM force field and the "round-robin" models RR1 and RR2

T (K)	P (kPa)	ρ_l (g/ml)				Hv (kJ/mol)			
		Expt.	RR1	RR2	TEAM	Expt.	RR1	RR2	TEAM
298	174.6	0.862	0.827	0.826	0.873	24.94	22.6	19.5	26.07
375	1432	0.737	0.705	0.666	0.740	19.91	17.74	13.37	20.87
420	3376	0.639	0.610	–	0.626	15.58	13.63	–	16.22

The vapor–liquid coexistence cannot be obtained which means this point falls outside of the vapor–liquid coexistence region.

listed in Appendix A. The parameterizations were conducted using DFF software package [9].

As required by the competition, a united-atom force field taken from the literature [3] was used as a "round-robin" model for comparisons. The "round-robin" model has two sets of LJ parameters which are denoted as RR1 and RR2 in this paper. The calculated liquid densities and heats of vaporization using both sets of parameters are compared with the experimental data [10] in Table 4. The results obtained using the RR1 parameters are closer to the experimental data than that obtained using the RR2 parameters. Therefore, we used the RR1 model for further comparisons in this work.

Monte Carlo (MC) simulations were extensively used in this work, mostly for gas phase or phase equilibrium studies. NPT MC simulations were performed mainly for vapor phase predictions. For the vapor–liquid equilibrium properties, Gibbs ensemble MC (GEMC) simulations were performed. Generally speaking, for a system that contains N_m molecules, each Monte Carlo cycle consists of N_m moves. These moves were divided into volume-change (for NPT and GEMC), particle-transfer (for GEMC), configuration, translation and rotation moves. The percentage volume-change moves in the total moves was 0.2% in GEMC and 1% in NPT MC; the number of particle-transfer moves was determined in such a way that roughly one accepted move for every 5–10 cycles (about 1–40% of the total number of moves depending on the temperatures), and the rest part was divided equally by other three moves. The VDW interactions were calculated using a cut-off of 12 Å and tail corrections. The Columbic interactions were calculated using the Ewald summation method. The MC simulations were performed with the software package MCCCS Towhee, version 4.16.8 [11].

Molecular dynamics (MD) simulations were performed mostly for liquid phases. In general, the time step was 1 fs in all simulation tasks. The Columbic integrations were treated with the particle mesh Ewald (PME) method. The cut-off value for the VDW interactions was 11 Å with standard tail corrections for energy and pressure. Both the temperatures and pressures were controlled using the Berendsen method. The MD simulations were carried out using GROMACS software package [12].

3. Results and discussion

3.1. VLE properties and the second virial coefficient

The vapor–liquid equilibrium properties were calculated using GEMC simulations. Each of the simulation processes was equilibrated for at least 100,000 cycles, followed by 100,000 cycles for data collection. Uncertainties were computed by breaking the total simulation into five blocks. A total of 266 molecules were put in the simulation boxes and the box sizes were set in such a way that the vapor phase contained at least 30 molecules.

The simulations were performed at 285, 325, 350, 375, 400 and 425 K. The saturated density scaling law and the law of rectilinear diameters [13] were used to estimate the critical properties T_c and ρ_c:

$$\rho_{liq} - \rho_{vap} = B(T - T_c)^{\beta} \quad (3)$$

$$1/2(\rho_{liq} + \rho_{vap}) = \rho_c + A(T - T_c) \quad (4)$$

The Clausius–Clapeyron equation was used to calculate the boiling point T_b from the vapor pressures:

$$\ln p = C + \frac{C'}{T} \quad (5)$$

In above equations, ρ_{liq} and ρ_{vap} are the saturated liquid and vapor densities obtained by GEMC simulations: A, B, C and C' are constants that can be determined by fitting the equations to the calculated data and β is the "critical exponent" parameter. The universal Ising value 0.325 [14] was used to calculate the critical properties

The second virial coefficient $B(T)$ was calculated using:

$$B(T) = -\frac{1}{2}\int \langle \exp(-U(r, \omega_1, \omega_2)/k_B T) - 1\rangle_{\omega_1,\omega_2} dR \quad (6)$$

where $U(r,\omega_1,\omega_2)$ is the potential energy of a pair of molecules with Euler angles ω_1, ω_2 and separated by r between two centers of mass. The ensemble average was taken by sampling different Euler angles generated by Monte Carlo simulations of 100,000 cycles. For every 20 cycles, two randomly oriented molecules were taken to calculate the energies of interaction with the separation between 1 and 1000 Å and at a 0.05-Å interval. The numerical integrations were performed using the trapezoid rule. Five independent runs were performed to estimate the uncertainty.

The calculated saturated vapor pressures, heats of vaporization, liquid and vapor densities and the second virial coefficients of ethylene oxide using both RR1 and TEAM force fields are summarized in Table 5. By comparing the calculated results with the experimental data [15] which were announced after the close of the IFPSC competition, the predictions using the TEAM force field are in excellent agreements with the experimental data, and significantly better than those predicted using the RR1 model.

In order to rigorously test the proposed models, the calculated vapor pressures, 1946 kPa for the RR1 model and 1415 kPa for the

Table 5
Comparisons of the experimental [15] and calculated VLE properties and the second virial coefficient of ethylene oxide at 375 K

Property	Expt.	Calc.	
		RR1	TEAM
T = 375 K			
P (kPa)	1437.1	1946 ± 42	1415 ± 54
Hv (kJ/mol)	19.95	17.74 ± 0.08	20.9 ± 0.1
ρ_l (g/ml)	0.744	0.705 ± 0.001	0.740 ± 0.003
ρ_g (g/ml)	0.024	0.034 ± 0.001	0.024 ± 0.001
B_2 (ml/mol)	−326	−262 ± 14	−322 ± 18
T_c (K)	469.15	464 ± 1	468 ± 1
ρ_c (g/ml)	0.314	0.319 ± 0.001	0.316 ± 0.001
T_b (K)	283.7	268 ± 3	285 ± 3

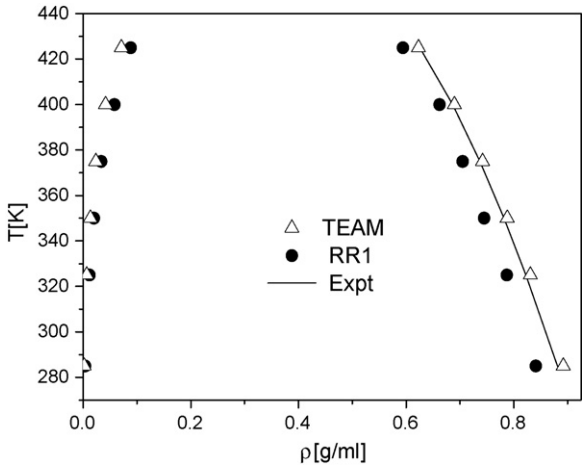

Fig. 3. Comparisons of the experimental [10] and calculated vapor–liquid coexistence densities of ethylene oxide using the RR1 and TEAM force fields.

TEAM force field at 375 K, were used for subsequent NPT ensemble simulations. This was based on an assumption that the predictions should be done without knowing any experimental data other than those used for optimizing the force field parameters.

The vapor–liquid coexistence curves are plotted in Fig. 3. The experimental data [10] for the liquid phase are available for comparison. The predicted liquid densities using the TEAM force field agree very well with the experimental data. From the coexistence curves, the critical temperature, the critical density and the normal boiling point of liquid ethylene oxide were calculated. The results obtained using different force fields are also listed in Table 5 and compared with the experimental data. The predictions using the TEAM force field are very close to the experimental data. It is of interest to note that the critical properties predicted using the RR1 model are in good agreement with the experimental result as well, despite significant errors in the predicted densities, heat of vaporization and vapor pressure.

3.2. Heat capacity

Constant pressure heat capacity (C_p) can be divided into the ideal gas (C_p^0) and residual (C_p^{res}) contributions:

$$C_p = \left(\frac{\partial\langle H\rangle}{T}\right)_p = \left(\frac{\partial\langle H^{id}\rangle}{T}\right)_p + \left(\frac{\partial\langle H^{res}\rangle}{T}\right)_p = C_p^0 + C_p^{res} \quad (7)$$

The ideal contribution, C_p^0, can be calculated using quantum chemistry method. The residual contribution, C_p^{res}, can be calculated using the fluctuation formula:

$$C_p^{res} = \frac{1}{k_B T^2}(\langle U^{res}H^{res}\rangle - \langle U^{res}\rangle\langle H^{res}\rangle) + \frac{P}{k_B T^2}(\langle VH^{res}\rangle - \langle V\rangle\langle H^{res}\rangle) - Nk_B \quad (8)$$

where, U^{res} is the intermolecular potential energy and $H^{res} = U^{res} + PV$ [16].

We calculated the ideal gas contribution using Gaussian03 program at the BLYP/6-31G(d) level of theory. A scaling factor of 0.9940 was applied to the calculated vibrational frequencies. For the residual contributions, NPT MC simulations were performed with 64 molecules for the gas phase and 216 molecules for the liquid phase. The simulations were equilibrated for at least 50,000 cycles and properties were averaged over 10^7 configurations divided into 10 blocks to estimate the standard deviations. Initially we performed these simulations with all degrees of freedom using the TEAM force field. Significantly deviations between the predicted and experimental data were obtained. After the IFPSC competition, we re-evaluated the procedure and realized that the intra-molecular vibrations must be excluded from the calculated residual enthalpies in the all-atom simulations. According to the literature [17], we carried out the simulation using rigid model in which all the intra-molecular degrees of freedom were fixed. The results, as given in Table 6, are in close agreement with the experimental data.

For comparison, we also calculated the heat capacity using the differentiation method. The residual enthalpies were calculated in a temperature range and then fitted to a polynomial expansion from which the analytic derivative (Eq. (7)) at specific temperature was calculated. At each temperature 1 million MC cycles were performed and the trajectory was divided into five blocks to estimate the standard deviations. Consistent results were obtained using the fluctuation and differentiation methods. It is worth mentioning that the RR1 model yields as good results as the TEAM model.

3.3. Isothermal compressibility

The isothermal compressibility can be calculated using the following equation:

$$\beta_T = -\frac{1}{\langle V\rangle}\left(\frac{\partial\langle V\rangle}{\partial P}\right)_T = \frac{1}{k_B T\langle V\rangle}(\langle V^2\rangle - \langle V\rangle^2) \quad (9)$$

Similar to the heat capacity, the isothermal compressibility can be calculated using the differentiation form and the volume fluctuation form.

We initially applied the differentiation method. The equilibrium P–V diagrams were obtained at 375 K using NPT MD for the liquid and NPT MC for the vapor. The MD simulations were performed with 343 molecules in the simulation box. The equilibration and production periods were 0.5 and 1.0 ns, respectively. The MC simulations were performed with 64 molecules in the simulation box, at least 100,000 cycles for the equilibration and 50,000 cycles for the data collection. The standard derivations were computed with five blocks. The calculated P–V curves are presented in Fig. 4 and the resulting isothermal compressibility are given in Table 7. For the vapor phase, the predicted value using the TEAM force field is very close to the experimental data while the result using the RR1 model is too low. The underestimate of RR1 model is consistent with the overestimated vapor pressure as stated above. For the liquid phase,

Table 6
The ideal gas (C_p^0), residual (C_p^r) and total heat of capacity (C_p) of saturated liquid and vapor ethylene oxide at 375 K (in J/(mol K))

Phase	Method	C_p^0	C_p^r		C_p		
			RR1	TEAM	RR1	TEAM	Expt. [15]
Gas	Fluctuation	58.957	16.5 ± 2.2	16.6 ± 1.3	75.5 ± 2.2	75.6 ± 2.2	73.56
	Differentiation		17.2 ± 0.5	17.2 ± 1.0	76.2 ± 0.5	76.2 ± 1.0	
Liquid	Fluctuation		46 ± 11.0	48.2 ± 7.6	105 ± 11	107.2 ± 7.6	101.32
	Differentiation		51.7 ± 0.8	52.2 ± 1.7	110.7 ± 0.8	111.2 ± 1.7	

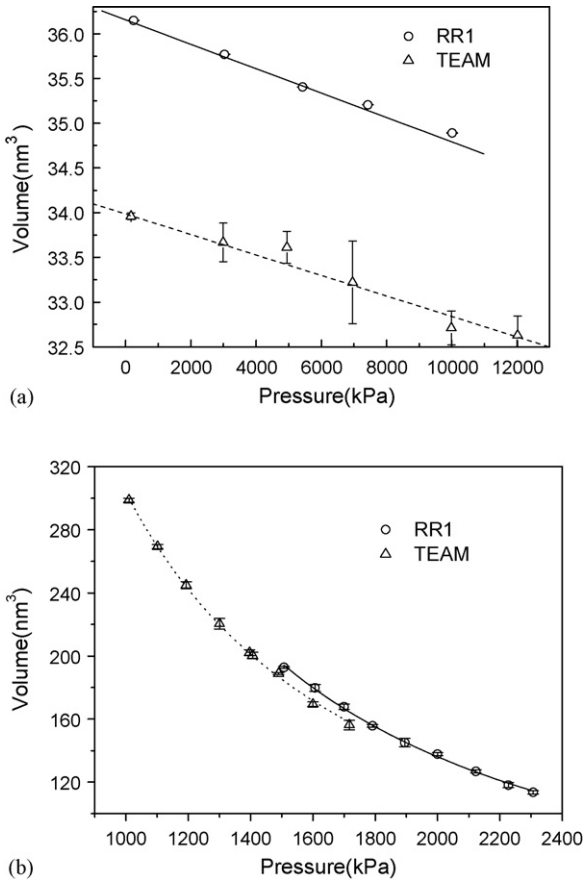

Fig. 4. Molar volumes as a function of pressures of ethylene oxide: (a) liquid; (b) gas.

the results obtained using both RR1 and TEAM models are similar and significantly larger than the reported experimental data.

After the IFPSC competition is closed, we applied the fluctuation method to calculate the isothermal compressibility using MC simulations for both liquid and vapor phases. The MC simulations were equilibrated for at least 50,000 cycles and averaged over 10^7 configurations which were divided into 10 blocks to estimate the standard deviations. The results, as listed in Table 7, are consistent with those of the differentiation method. Considering the fact that the force field performs consistently well in many other predictions as presented in this paper, we suggest that the experimental data for the liquid isothermal compressibility should be re-evaluated.

3.4. Surface tension

The surface tension was derived from the pressure tensors:

$$\gamma_0 = \frac{1}{2}L_z\left[P_{zz} - \frac{1}{2}(P_{xx} + P_{yy})\right] \tag{10}$$

where L_z is the box length in the z-direction. In order to obtain stable vapor–liquid interface, NVT MD simulation was performed on a slab of 686 ethylene oxide molecules in a fixed box of 3.24 nm × 3.24 nm × 16.0 nm. The system was equilibrated for 1 ns and data collection for 1 ns. The error bars were computed from five independent simulations.

Table 7
Comparisons of the experimental [15] and the calculated isothermal compressibility (10^{-6} kPa^{-1}) of ethylene oxide at 375 K

Phase	Expt.	Differentiation		Fluctuation	
		RR1	TEAM	RR1	TEAM
Gas	819	639 ± 22	858 ± 26	677 ± 47	844 ± 51
Liquid	2.6	3.6 ± 0.4	3.5 ± 0.1	3.9 ± 0.7	3.3 ± 0.5

Table 8
Comparisons of the experimental [15] and the calculated surface tension of liquid ethylene oxide at 375 K

Phase	γ (N/m)		
	Expt.	RR1	TEAM
Liquid	0.012	0.0073 ± 0.0006	0.011 ± 0.003

The calculated values of surface tension at 375 K were listed in Table 8. The calculated liquid phase surface tension using the TEAM force field agree very well with the experimental value and is significantly more accurate than that obtained using the RR1 model.

3.5. Viscosity

The shear viscosities of liquid ethylene oxide were simulated using the periodic perturbation method [18], a non-equilibrium molecular dynamics (NEMD) method. In this method, simulations are carried out in 3D periodic cells in a way similar to normal molecular dynamics simulations. A periodic external force $a(z)$, which is a function of the z-direction, is applied in the x-direction on each of the particles.

$$a_x(z) = \Lambda\cos(kz) \tag{11}$$

where the amplitude Λ is the strength of the perturbation. According to Navier–Stokes equation, a velocity profile is built up when the system reaches steady state:

$$u_x(z) = V\cos(kz) \tag{12}$$

From which the shear viscosity can be estimated:

$$\eta = \frac{\Lambda}{V}\frac{\rho}{k^2} \tag{13}$$

The viscosity obtained depends on the shear rate Λ of the acceleration profile in a complex way. The shear rate should be small enough so that the perturbation does not disturb the equilibrium of the system. On the other hand, small force leads to low signal–noise ratio. We have developed a linear extrapolation scheme [19] to estimate the "undisturbed" shear viscosity.

The liquid simulation box contains 343 molecules. The system was equilibrated for at least 2 ns and then 1 ns NEMD simulations were carried out for the data collection. Four (4) acceleration amplitudes (Λ) 0.01, 0.02, 0.03, 0.04 nm ps^{-2} were performed. At each point, the uncertainty was estimated using the block average method and its reverse was used as the weighting factor for fitting the data to a straight line. The root mean square deviation of the fit was interpreted as the uncertainty for the extrapolated viscosity.

For the vapor phase, the NEMD method does not work well due to the weak intermolecular forces. The viscosity was calculated using equilibrium molecular dynamics and Einstein relation.

$$\eta = \lim_{t\to\infty}\frac{1}{2}\frac{V}{k_BT}\frac{\mathrm{d}}{\mathrm{d}t}\left\langle\left(\int_{t_0}^{t_0+t}P_{xz}(t')\,\mathrm{d}t'\right)^2\right\rangle_{t_0} \tag{14}$$

NVT MD simulations were constructed with 64 molecules in a cubic box with full periodical boundary condition. The initial configuration was equilibrated for 5 ns and the data collection period was 10 ns. The uncertainty was estimated using the block average method.

The calculated values of viscosities of ethylene oxide at 375 K using MD simulations were listed in Table 9. The liquid viscosi-

Table 9
Comparisons of the experimental [15] and the calculated gas and liquid viscosities of ethylene oxide at 375 K

Phase	η (10^{-4} Pa s)		
	Expt.	RR1	TEAM
Gas	0.124	0.079 ± 0.006	0.204 ± 0.006
Liquid	1.51	1.186 ± 0.054	1.49 ± 0.064

ties were extrapolated as illustrated in Fig. 5. The calculated liquid phase viscosity using the TEAM force field is in close agreement with the experimental data, and significantly more accurate than that obtained using the RR1 model. But for the vapor phase the prediction is poor. This could be due to the inefficiency of the equilibrium method. Further investigation is required in order to fully understand what causes this discrepancy.

3.6. Thermal conductivity

Thermal conductivities of ethylene oxide were estimated using the reverse non-equilibrium molecular dynamics (RNEMD) method which was explained in detail by Müller-Plathe [20]. For completeness, a brief summary is given here.

Macroscopically, the thermal conductivity λ is defined by:

$$\mathbf{J} = -\lambda \nabla T \tag{15}$$

where ∇T is the gradient of the temperature T, $\mathbf{J}$ is the resulting heat flux vector which is defined as the amount of energy transferred in a unit time through a surface of a unit area. In an isotropic fluid, the temperature gradient and the heat flux are in the same direction and λ is a scalar.

If x is the direction of the temperature gradient, the thermal conductivity can be defined microscopically in terms of time averages:

$$\lambda = -\lim_{\partial T/\partial x \to 0} \lim_{t \to \infty} \frac{\langle J_x(t) \rangle}{\langle \partial T/\partial x \rangle} \tag{16}$$

Since $J_x(t)$ is a quantity with large fluctuation, its average converges slowly.

In the RNEMD simulation, a heat flux is imposed on the system and the resulting temperature gradient is measured. The advantage is that the slowly converging quantity (heat flux) is known exactly and it does not need to be calculated. The temperature and its gradient, on the other hand, are averaged over time as well as over many particles so that they converge rapidly.

In order to impose a heat flux and to calculate a temperature profile, the simulation box is divided into N slabs perpendicular to the x-direction. Slab 0 is defined as the "cool" slab and slab $N/2$ is defined as the "hot" slab. The instantaneous local kinetic temperature T_k in slab k is given by

$$T_k = \frac{1}{3n_k k_B} \sum_{i \in k}^{n_k} m_i v_i^2 \tag{17}$$

where the sum goes over n_k atoms in the slab; m_i is the mass of atom i, and v_i is its velocity; k_B is Boltzmann's constant. The heat flux is generated by exchanging the velocities of atoms in the cool and hot slabs so that the temperature increases in the hot slab and decreases in the cool slab. In the simulation the velocities of the hottest atom of the cool slab and the coldest atom of the hot slab were exchanged. If the hottest atom in cool slab has a lower temperature than that of the coolest atom in the hot slab, the exchange does not occur. The exchange produces an energy transfer from the cool slab to the hot slab, which leads to a temperature difference between the cool and the hot slabs and a temperature gradient in the region between the two slabs.

After reaching a steady state, the energy transfer imposed by the velocity exchange is balanced by the heat flux in the opposite direction. The temperature gradient in the steady state depends on the thermal conductivity. The thermal conductivity is then calculated from:

$$\lambda = -\frac{\sum_{\text{transfers}} m/2(v_h^2 - v_c^2)}{2tL_yL_z\langle \partial T/\partial x \rangle} \tag{18}$$

The sum is taken over all transfer events during the simulation time t. The subscripts h and c refer to the hot and the cold particle of identical mass m whose velocities are interchanged. The factor of 2 in the denominator arises from the periodicity of the arrangement of slabs in simulation box.

In this work, the thermal conductivities were calculated for both the saturated liquid and vapor phases. The box lateral lengths in x-, y- and z-directions were specified as 3:1:1. The actual box sizes were determined by the corresponding densities obtained from the NPT simulations and number of molecules in the simulation box. A total of 1029 molecules were included for the liquid simulation and 192 molecules for the vapor. The data collection stages were chosen from 0.2 to 1.0 ns, and the instantaneous temperature was calculated every 100 steps. The RNEMD method was implemented for all atom force field based on GROMACS 3.3.1. Due to time constraints, we did not implement the united atom mode.

The frequency of the energy exchange, which corresponds to the imposed heat flux, is a critical factor to be considered. In this work we tested the energy exchange frequencies by comparing the calculated results with the results reported in the literature [21]. The optimal values are 1/500 fs^{-1} for liquid 1/2000 fs^{-1} for gas. The

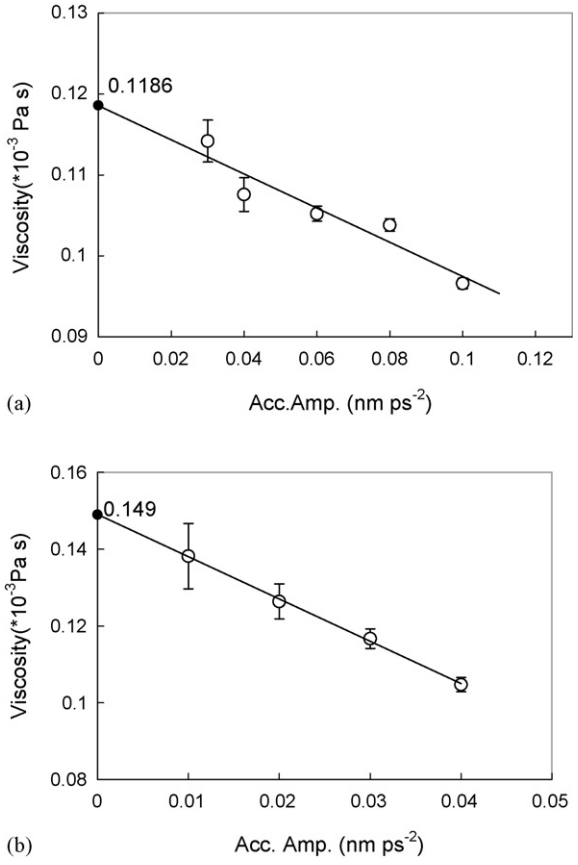

Fig. 5. Calculated liquid viscosity of ethylene oxide by NEMD simulations using the RR1 and TEAM force fields.

Table 10
Comparisons of the experimental [15] and the calculated liquid and vapor thermal conductivities of ethylene oxide at 375 K using TEAM force field

Phase	Ex. Freq. (fs^{-1})	λ ($W m^{-1} K^{-1}$)	
		Expt.	Calc.
Vapor	1/2000	0.0204	0.026 ± 0.002
Liquid	1/500	0.12	0.238 ± 0.009

results obtained using the TEAM force field are listed in Table 10. Unfortunately the predictions were not very satisfactory, especially for the liquid phase. Based on our latest work on the heat capacity as explained above, we believe the intra-molecular motions must be treated quantum mechanically in these calculations. A simple solution is to remove the intra-molecular degree of freedom from the classical simulations [17]. We are conducting further researches along this direction.

4. Conclusion

In this work, a TEAM force field in the AMBER form was developed and applied with MD and MC simulation methods to predict various thermodynamic properties of liquid and vapor ethylene oxide. Although the force field is developed using a few basic data—the *ab initio* energetic data and empirical liquid data at a few selected data points, the force field performs reasonably well for predicting a broad range of properties including phase separation, surface tension, heat capacity, isothermal compressibility, viscosity and thermo-conductivity. This is very encouraging because it demonstrates that a general force field can be transferable in predicting very different properties.

The quality of the present force field can be further improved. For example, there is clearly a polarization effect (the molecular dipole moment increases 17% from gas to liquid) for the ethylene oxide molecule. In this work we have simply ignored the gas phase and focused on the liquid phase for the parameterization.

Some of the predictions made in this work are not accurate in comparison with the experimental data. In specific, the calculated isothermal compressibility of the liquid, viscosity of the vapor and the thermal conductivity are in large deviations, roughly 27, 65 and 100%, respectively, from the experimental data. Other than the force field quality that requires further work as mentioned above, great attention should be focused on the simulation methods. For example, the RNEMD method for predicting viscosity and thermo-conductivity are of great interest for further investigations.

Acknowledgments

Financial support from the Chinese Nature Science Foundation (No. 20473052, No. 10676021) and National Basic Research Program of China (2003CB615804, 2007CB209700) is gratefully acknowledged.

Appendix A. The force field parameters

A.1. The RR model

Model	Type	σ (Å)	ε/k_B (K)
RR1	CH_2–CH_2	3.7143	90.0
	O–O	2.6666	73.0
RR2	CH_2–CH_2	3.5950	72.0
	O–O	2.8000	90.58

A.2. The TEAM model

Bond type	b_0 (Å)	k_b (kJ/mol)
C–C	1.5162	1413.893
C–O	1.3965	1118.79
C–H	1.0894	1569.242

Angle type	θ_0 (°)	k_θ (kJ/mol)
C–C–O	106.8885	22.8472
C–C–H	118.9215	135.4181
O–C–H	115.7252	191.6439
H–C–H	116.0000	84.2231
C–O–C	36.3433	152.7461

Bond increment	δ_{ij} (e)
C–C	0.0000
C–H	−0.117
C–O	0.1585

LJ12-6	R^0 (Å)	ε (kJ/mol)
C	3.7989	0.5062
O	3.5215	0.6520
H	2.6070	0.0360

Charge	(e)
O	−0.3216
CH_2	0.1608

References

[1] TEAM is an all-atom force field that is under development in our research group. There are several publications related to one or a few compounds:
(a) H. Sun, Fluid Phase Equilib. 217 (2004) 59–76;
(b) C. Wu, X. Li, J. Dai, H. Sun, Fluid Phase Equilib. 236 (2005) 66–77;
(c) J. Dai, C. Wu, X. Bao, H. Sun, Fluid Phase Equilib. 236 (2005) 78–85.
[2] For more information about the Industrial Fluid Property Simulation Challenge, see http://fluidproperties.org/challenge/4th/announcement.
[3] P.A. Wielopolski, E.R. Smith, Mol. Phys. 54 (1985) 467–478.
[4] M. Krishnamurthy, S. Murad, J.D. Olson, Mol. Simul. 32 (2006) 11–16.
[5] R.D. Mountain, J. Phys. Chem. B 109 (2005) 13352–13355.
[6] M.J. Frisch, G.W. Trucks, H.B. Schlegel, G.E. Scuseria, M.A. Robb, J.R. Cheeseman, J.A. Montgomery Jr., T. Vreven, K.N. Kudin, J.C. Burant, J.M. Millam, S.S. Iyengar, J. Tomasi, V. Barone, B. Mennucci, M. Cossi, G. Scalmani, N. Rega, G.A. Petersson, H. Nakatsuji, M. Hada, M. Ehara, K. Toyota, R. Fukuda, J. Hasegawa, M. Ishida, T. Nakajima, Y. Honda, O. Kitao, H. Nakai, M. Klene, X. Li, J.E. Knox, H.P. Hratchian, J.B. Cross, V. Bakken, C. Adamo, J. Jaramillo, R. Gomperts, R.E. Stratmann, O. Yazyev, A.J. Austin, R. Cammi, C. Pomelli, J.W. Ochterski, P.Y. Ayala, K. Morokuma, G.A. Voth, P. Salvador, J.J. Dannenberg, V.G. Zakrzewski, S. Dapprich, A.D. Daniels, M.C. Strain, O. Farkas, D.K. Malick, A.D. Rabuck, K. Raghavachari, J.B. Foresman, J.V. Ortiz, Q. Cui, A.G. Baboul, S. Clifford, J. Cioslowski, B.B. Stefanov, G. Liu, A. Liashenko, P. Piskorz, I. Komaromi, R.L. Martin, D.J. Fox, T. Keith, M.A. Al-Laham, C.Y. Peng, A. Nanayakkara, M. Challacombe, P.M.W. Gill, B. Johnson, W. Chen, M.W. Wong, C. Gonzalez, J.A. Pople, Gaussian 03., Gaussian, Inc., Pittsburgh, PA, 2003.
[7] D.R Lide, CRC Handbook of Chemistry and Physics, CRC Press, Boca Raton, FL, 1995.
[8] NIST Chemistry WebBook, NIST Standard Reference Database Number 69, National Institute of Standards and Technology, Gaithersburg, MD, June 2005, http://webbook.nist.gov.
[9] DFF (Direct Force Field™) is a software package that can be used to derive parameters from ab initio and empirical data. It is developed and licensed Aeon Technology, Inc., San Diego, CA, USA, 2004.
[10] C.L. Yaws, Chemical Properties Handbook, The McGraw-Hill Companies, Inc., New York, 1999.
[11] MCCCS Towhee is a Monte Carlo molecular simulation program. More information is available at http://towhee.sourceforge.net.
[12] D. van der Spoel, E. Lindahl, B. Hess, G. Groenhof, A.E. Mark, H.J. Berendsen, J. Comp. Chem. 26 (2005) 1701–1718.

[13] M.G. Martin, J.I. Siepmann, J. Phys. Chem. B 102 (1998) 2569–2577.
[14] B. Chen, J.J. Potoff, J.I. Siepmann, J. Phys. Chem. B 105 (2001) 3093–3104.
[15] The experimental data were published by the IFPSC committee and can be found at http://fluidproperties.org/4th-challenge-results.
[16] M. Lagache, P. Ungerer, A. Boutin, A.H. Fuchs, Phys. Chem. Chem. Phys. 3 (2001) 4333–4339.
[17] E. Lussetti, T. Terao, F. Müller-Plathe, J. Phys. Chem. B 111 (2007) 11516–11523.
[18] B. Hess, J. Chem. Phys. 116 (2002) 209–217.
[19] L. Zhao, X. Wang, L. Wang, H. Sun, Fluid Phase Equilib. 260 (2007) 212–217.
[20] F. Müller-Plathe, J. Chem. Phys. 106 (1997) 6082–6085.
[21] M. Zhang, E. Lussetti, L.E.S. de Souza, F. Müller-Plathe, J. Phys. Chem. B 109 (2005) 15060–15067.